

Aliasing-Free Neural Audio Synthesis

Yicheng Gu, *Student Member, IEEE*, Junan Zhang, Chaoren Wang, Jerry Li, Zhizheng Wu, *Senior Member, IEEE*, Lauri Juvela, *Senior Member, IEEE*

Abstract—Neural vocoders and codecs reconstruct waveforms from acoustic representations, which directly impact the audio quality. Among existing methods, upsampling-based time-domain models are superior in both inference speed and synthesis quality, achieving state-of-the-art performance. Still, despite their success in producing perceptually natural sound, their synthesis fidelity remains limited due to the aliasing artifacts brought by the inadequately designed model architectures. In particular, the unconstrained nonlinear activation generates an infinite number of harmonics that exceed the Nyquist frequency, resulting in “folded-back” aliasing artifacts. The widely used upsampling layer, ConvTranspose, copies the mirrored low-frequency parts to fill the empty high-frequency region, resulting in “mirrored” aliasing artifacts. Meanwhile, the combination of its inherent periodicity and the mirrored DC bias also brings “tonal artifact,” resulting in constant-frequency ringing. This paper aims to solve these issues from a signal processing perspective. Specifically, we apply oversampling and anti-derivative anti-aliasing to the activation function to obtain its anti-aliased form, and replace the problematic ConvTranspose layer with resampling to avoid the “tonal artifact” and eliminate aliased components. Based on our proposed anti-aliased modules, we introduce Pupu-Vocoder and Pupu-Codec, and release high-quality pre-trained checkpoints to facilitate audio generation research. We build a test signal benchmark to illustrate the effectiveness of the anti-aliased modules, and conduct experiments on speech, singing voice, music, and audio to validate our proposed models. Experimental results confirm that our lightweight Pupu-Vocoder and Pupu-Codec models can easily outperform existing systems on singing voice, music, and audio, while achieving comparable performance on speech. Demos, codes, and checkpoints are available at <https://www.yichenggu.com/AliasingFreeNeuralAudioSynthesis/>.

Index Terms—neural codec, neural vocoder, speech synthesis, singing voice synthesis, audio synthesis, DDSP, anti-aliasing.

I. INTRODUCTION

EXISTING audio generation systems typically consist of two stages. Firstly, an acoustic model [1–3] converts human inputs into an intermediate representation. Then, a decoder model, often referred to as a vocoder, reconstructs the waveform from the representation. Among different types of vocoders, the neural network-based ones [4–18] are essential due to their superior synthesis quality compared with the DSP-based ones [19–21]. Historically, the development of the neural vocoder has primarily focused on time-domain models, which directly generate waveforms by upsampling from the acoustic representations without explicitly modeling the phase. These models include flow-based [7–9], diffusion-based [10–12], auto-regressive (AR)-based [4–6], differentiable digital signal processing (DDSP)-based [13–15], and generative adversarial network (GAN)-based vocoders [16–18].

Yicheng Gu and Jerry Li are with the Spellbrush, Akihabara, Tokyo, Japan.

Yicheng Gu and Lauri Juvela are with the Acoustic Lab, Department of Information Communications Engineering, Aalto University, Espoo, Finland.

Yicheng Gu, Junan Zhang, Chaoren Wang, and Zhizheng Wu are with the Chinese University of Hong Kong, Shenzhen, Guangdong, China.

Among these various approaches, GAN-based vocoders are extensively studied due to their faster inference speed and higher synthesis quality. Following these developments, GAN-based neural audio codecs [22–24] have also been proposed in recent years. The main idea of the neural audio codec is to decompose the continuous intermediate representation into discrete tokens via an encoder and vector quantization [25–27], which can later be transformed back and fed to a vocoder-like decoder to obtain the sound. Such a discretization facilitates the use of large language models, resulting in state-of-the-art (SOTA) audio generation systems [1–3].

Although these upsampling-based time-domain models can generate perceptually natural sound, recent studies suggest that their synthesis fidelity remains limited due to aliasing artifacts brought by inadequately designed model architectures [28–31]. Specifically, the unconstrained nonlinear activation generates infinitely many harmonics that exceed the Nyquist frequency, resulting in “folded-back” aliasing artifacts [16, 31]. The widely used upsampling layer, ConvTranspose, copies the mirrored low-frequency parts to fill the empty high-frequency region, resulting in “mirrored” aliasing artifacts [28–30]. Meanwhile, the combination of its inherent periodicity and the mirrored DC bias also introduces “tonal artifact” [28–30], resulting in constant-frequency ringing. Several recent works have been proposed to address these issues, but at the cost of either synthesis speed [16] or quality degradation [28–30]. Others attempt to use the aliasing-free time-frequency (TF) domain model as an alternative [31–33], which generates TF representations (TFRs) and uses their inverse transforms to obtain the waveform; but their synthesis quality remains limited due to the difficulty in explicitly modeling the phase.

This paper aims to address these problems inherent in activation and upsampling modules from a signal processing perspective. Specifically, we apply oversampling and anti-derivative anti-aliasing (ADAA) techniques [34–39] to the activations to obtain their anti-aliased form, and replace the ConvTranspose layer with resampling to avoid “tonal artifact” and eliminate aliased components. Based on our proposed anti-aliased modules, we introduce Pupu-Vocoder and Pupu-Codec, and release high-quality pre-trained checkpoints to facilitate audio generation research. We build a test signal benchmark to illustrate the effectiveness of the anti-aliased modules, and conduct experiments on speech, singing voice, music, and audio to validate our proposed models. Experimental results confirm that our lightweight Pupu-Vocoder and Pupu-Codec models can easily outperform existing systems on singing voice, music, and audio, while achieving comparable results on speech. Beyond audio synthesis, we emphasize that our method is domain-agnostic, making it applicable to other domains where aliasing is a concern, such as image generation.

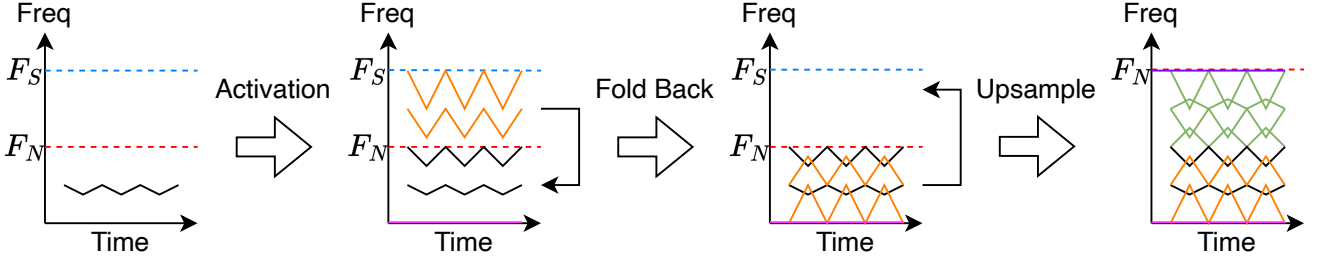


Fig. 1: Illustration of different aliasing artifacts brought by the activation functions and upsampling layers. F_S denotes the sampling rate, F_N denotes the Nyquist frequency. The colored contours represent “folded-back” aliasing artifacts (orange), “mirrored” aliasing artifacts (green), DC bias (pink), and “tonal artifact” (purple), respectively.

II. THEORETICAL BACKGROUND

In this section, we discuss the related work and outline the theoretical background of the “folded-back” and “mirrored” aliasing artifacts, as well as the “tonal artifact” introduced by the activation functions and upsampling layers.

A. Artifacts due to Non-Linear Activation Functions

Applying an unconstrained activation to a discrete signal will generate an infinite number of harmonics that exceed the Nyquist frequency. According to the Nyquist–Shannon sampling theorem [40], these harmonics will then be “folded-back” and become aliasing artifacts, as illustrated in Figure 1.

Following WaveHax [31], we take the ReLU activation as an example to better illustrate the idea. Suppose the input signal is a sine wave with angular frequency ω for continuous time $t \in R$, after applying the ReLU activation function, the resulting signal’s Fourier expansion becomes:

$$\text{ReLU}(\sin(\omega t)) = \frac{1}{\pi} + \frac{\sin(\omega t)}{2} - \sum_{k=1}^{\infty} \frac{2 \cos(2k\omega t)}{\pi(2k-1)(2k+1)}, \quad (1)$$

where the last term induces an infinite amount of harmonics. The frequency components higher than the Nyquist frequency, where $\frac{k\omega}{\pi} > \frac{F_N}{2}$, would become the aliasing artifacts.

To address this issue, StyleGAN 3 [41] and BigVGAN [16] utilize the oversampling technique to temporarily increase the Nyquist frequency before applying the activation, thus reducing the amount of aliased components. To implement such a technique, upsample the signal with a low-pass filter before applying the activation, and then downsample it back with a low-pass filter to remove the extra frequency region, as:

$$\begin{aligned} \hat{x} &= \text{lowpass}(\text{upsample}(x, c), F_N), \\ y &= \text{downsample}(\text{lowpass}(f(\hat{x}), F_N), c), \end{aligned} \quad (2)$$

where x is the input signal, \hat{x} is the upsampled signal, y is the output signal, $f(\cdot)$ is the activation function, F_N is the Nyquist frequency which is the half of the sampling rate F_S , $\text{lowpass}(x, F_N)$ represents low-pass filtering with a cut-off frequency of F_N , $\text{upsample}(x, c)$ and $\text{downsample}(x, c)$ denotes upsampling or downsampling the input signal by a factor of c . To effectively eliminate the aliased components, an oversampling factor of 4 or 8 is typically required [34], which makes the signal excessively long and thus incompatible with deep learning applications due to GPU memory constraints.

To avoid these issues, several more advanced anti-aliasing techniques have been proposed. For instance, a harmonic mixed model can be used for polynomial nonlinearities [42], or a non-linearity can be approximated using a filter bank model [43]. However, such methods are usually complex and limited to a few function types, excluding the widely used activations. Recently, a simple yet effective method called ADAA [34–39] has been proposed. Its main idea is to convert the discrete signal to a continuous one before applying the activation function. Since the signal is continuous, there are no sampling frequency constraints, and therefore, no aliasing artifacts. Such a signal can then be low-pass filtered to remove the extra frequency region and resampled back. Specifically, suppose we have a signal x for continuous time $t \in [0, n]$:

$$\tilde{x}(t) = \begin{cases} x_1 + \tau(x_0 - x_1), & \text{if } 0 \leq |t| < 1 \\ \vdots \\ x_n + \tau(x_{n-1} - x_n), & \text{if } n-1 \leq |t| < n \end{cases} \quad (3)$$

where \tilde{x} is a continuous signal and $\tau = 1 - (t \bmod 1)$ is a time variable that runs 1...0 between each sample. Applying the activation $f(\cdot)$ to the signal \tilde{x} , followed by low-pass filtering with a filter kernel $h(\cdot)$ and discrete resampling, gives:

$$y_t = \int_{-\infty}^{\infty} h(u) f(\tilde{x}(t-u)) du, \quad (4)$$

where $h(\cdot)$ is a rectangular filter kernel with unit width:

$$h(t) = \begin{cases} 1, & \text{if } 0 \leq t \leq 1 \\ 0, & \text{otherwise} \end{cases} \quad (5)$$

Following the derivations in [35], the integral in Equation 4 can be reduced to a closed-form expression as follows:

$$y_t = \frac{F(x_t) - F(x_{t-1})}{x_t - x_{t-1}}, \quad (6)$$

where $F(\cdot)$ is the first order anti-derivative of $f(\cdot)$. Notably, the standard ADAA often suffers from numerical instability due to the denominator, and a tolerance level (TOL) is usually needed to disable ADAA when the denominator is small:

$$y_t = f\left(\frac{x_t + x_{t-1}}{2}\right), \quad \text{if } |x_t - x_{t-1}| < \text{TOL} \quad (7)$$

In contrast to this general formulation, the ADAA form derived from our adopted SnakeBeta [44] activation completely avoids this problem, as it contains no denominator terms and thus ensures numerical stability without threshold-based switching.

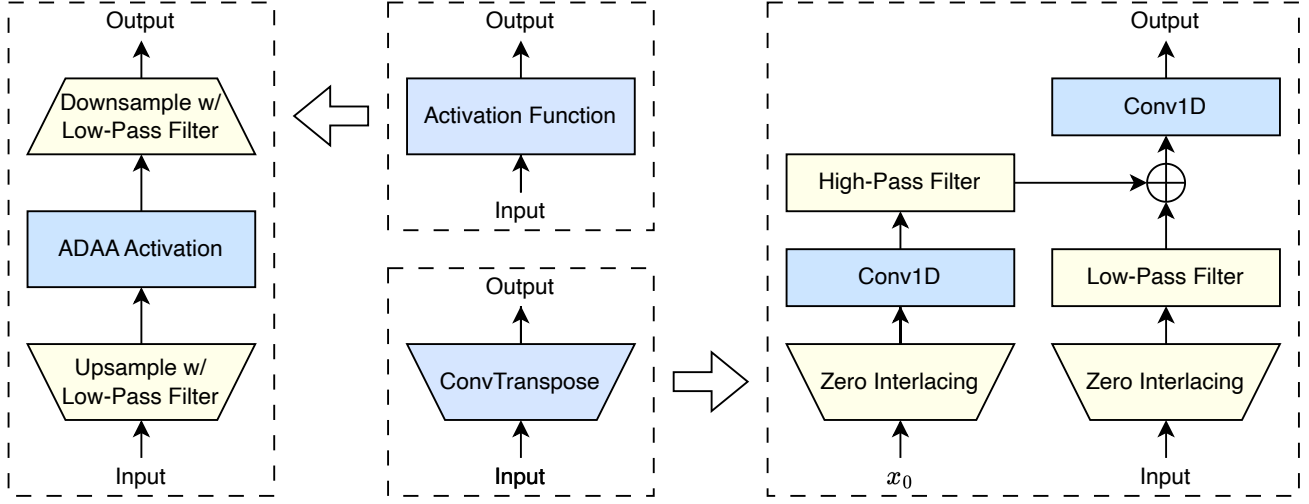


Fig. 2: The main idea of our proposed anti-aliased activation function and upsampling layer. “ \rightarrow ” means “replacing the original inadequately designed model architecture with our proposed artifacts-free modules”. x_0 is the latent representation obtained from the first Conv1D layer in the decoder. We employ a resampling layer (zero-interlacing + low-pass filtering) with a noise-like, high-pass filtered deterministic prior, obtained from the zero-interlaced x_0 , to replace the problematic ConvTranspose layer. Additionally, we utilize an oversampled ADAA activation function to replace the original unconstrained one.

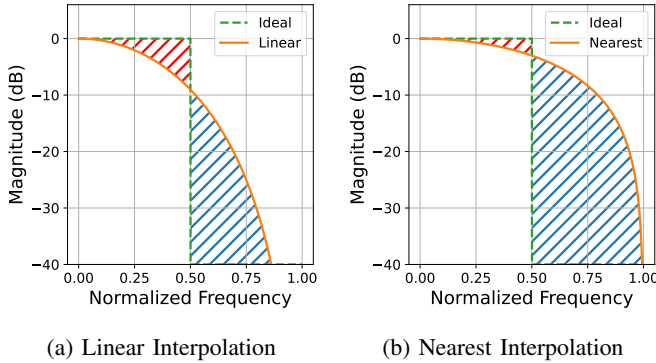


Fig. 3: Illustration of the equivalent filter frequency responses of linear and nearest interpolations. The orange contour and green dashed line represent the actual and ideal frequency responses, respectively. The red hatched area indicates the attenuation of the valid frequency region we want to retain, while the blue hatched area highlights the residual “mirrored” aliasing artifacts that the interpolation layer fails to remove.

B. Artifacts due to Upsampling Layers

The widely used upsampling layer, ConvTranspose, zero-interlaces the input signal and applies convolution afterwards. In the frequency domain, as illustrated in Figure 1, this process can be viewed as copying the mirrored low-frequency parts to fill the empty high-frequency region, resulting in “mirrored” aliasing artifacts. The ConvTranspose layer also suffers from the “tonal artifact”, manifested as constant-frequency ringing, as shown in Figure 1. Such a phenomenon originates from two sources. Firstly, the DC bias introduced by non-linear activations or network bias parameters is mirrored into high-frequency bands; meanwhile, the computational process of ConvTranspose has an inherent periodicity due to its fixed stride and shared weights, introducing constant-frequency ringing at the same locations as the mirrored DC bias [29].

To address these problems, a low-pass filter can be adapted after the ConvTranspose layer to eliminate the aliased parts. To compensate for the training instability brought by the filter, a noise-like, high-pass filtered deterministic prior can be utilized to fill the empty high-frequency region [30]. This strategy effectively removes the “mirrored” aliasing artifacts, but leaves the “tonal artifact” unaddressed. To resolve the “tonal artifact”, previous studies [28, 29] propose to replace the problematic ConvTranspose layer with the linear and nearest interpolations, since they do not exhibit inherent periodicity and their operations are equivalent to low-pass filtering, which can simultaneously remove the mirrored DC bias in the high-frequency region. However, such a replacement does not effectively eliminate the “mirrored” aliasing artifacts, and it will also introduce “filter artifact” due to their poor filter frequency responses, resulting in a degradation of quality. Specifically, the linear and nearest interpolations are equivalent to convolving the signal with low-pass filter kernels, as:

$$h_{\text{linear}}(t) = \begin{cases} 1 - \left| \frac{t}{N} \right|, & \text{if } |t| \leq N \\ 0, & \text{otherwise} \end{cases} \quad (8)$$

$$h_{\text{nearest}}(t) = \begin{cases} 1, & \text{if } |t| \leq N \\ 0, & \text{otherwise} \end{cases}$$

where $2N + 1$ is the kernel length. The comparison between the ideal and equivalent filter frequency responses is illustrated in Figure 3. It can be observed that the frequency responses of these interpolation layers deviate significantly from the ideal rectangular window. In particular, the slow roll-off in the pass-band causes an attenuation of the valid frequency region that should be preserved, represented by the red hatched regions. Meanwhile, the insufficient suppression in the stop-band fails to eliminate the “mirrored” aliasing artifacts, indicated by the blue hatched regions. This phenomenon, where the filter fails to preserve the valid frequency region while incompletely removing aliasing artifacts, is known as the “filter artifact.”

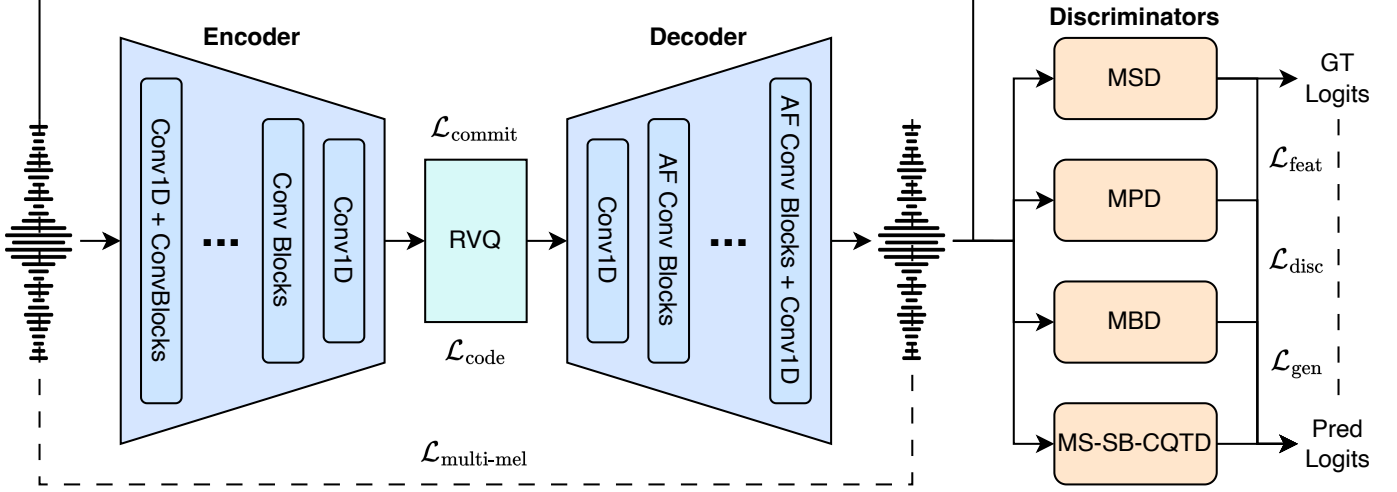


Fig. 4: Architecture and training schemes of the proposed models. The Pupu-Codec consists of an encoder, a residual vector quantizer (RVQ) module, a decoder, and four different discriminators. “AF Conv Blocks” are obtained by modifying the convolution blocks used in BigVGAN [16] and DAC [23] with our proposed anti-aliased activation and upsampling modules. Replacing the waveform input, encoder, and RVQ module with a mel-spectrogram as the input gives the Pupu-Vocoder model.

III. METHODOLOGY

In this section, we illustrate our idea for obtaining the anti-aliased activation and upsampling modules based on the theoretical analysis in Section II, as shown in Figure 2.

A. Anti-Aliased Activation Functions

The architecture of the proposed anti-aliased activation function is shown in Figure 2. We use the oversampling [16] technique and apply ADAA [34–39] to the activation function. Specifically, we use the SnakeBeta [44] activation function to utilize its advantage in modeling the audio’s periodic nature, following [16, 23]. In particular, the SnakeBeta activation is:

$$f(x) = x + \frac{\sin^2(\alpha x)}{\beta}, \quad (9)$$

where α and β are learnable parameters. Integrating the equation gives its first-order anti-derivative:

$$F(x) = \frac{x^2}{2} + \frac{x}{2\beta} - \frac{\sin(2\alpha x)}{4\alpha\beta} + C, \quad (10)$$

where C is a constant. Applying ADAA gives:

$$y_t = \frac{\left(\frac{x_t^2}{2} + \frac{x_t}{2\beta} - \frac{\sin(2\alpha x_t)}{4\alpha\beta}\right) - \left(\frac{x_{t-1}^2}{2} + \frac{x_{t-1}}{2\beta} - \frac{\sin(2\alpha x_{t-1})}{4\alpha\beta}\right)}{x_t - x_{t-1}}, \quad (11)$$

which can be simplified with the sum-to-product formula, as:

$$\sin(2\alpha x_t) - \sin(2\alpha x_{t-1}) = 2 \cos(\alpha(x_t + x_{t-1})) \sin(\alpha(x_t - x_{t-1})) \quad (12)$$

which can be substituted back to obtain the following:

$$y_t = \frac{(x_t - x_{t-1})(x_t + x_{t-1})}{2(x_t - x_{t-1})} + \frac{x_t - x_{t-1}}{2\beta(x_t - x_{t-1})} - \frac{\cos(\alpha(x_t + x_{t-1})) \sin(\alpha(x_t - x_{t-1}))}{2\alpha\beta(x_t - x_{t-1})}, \quad (13)$$

where each numerator can either eliminate or absorb the denominator, giving the following closed form:

$$y_t = \frac{1}{2\beta} + \frac{x_t + x_{t-1}}{2} - \frac{\cos(\alpha(x_t + x_{t-1})) \sin(\alpha(x_t - x_{t-1}))}{2\beta}, \quad (14)$$

which yields our ADAA SnakeBeta. As we mentioned in Section II, such a function eliminates the denominator entirely, ensuring numerical stability without the need for threshold-based switching in standard ADAA. Meanwhile, it also has bounded outputs for bounded inputs since all $\sin(\cdot)$, $\cos(\cdot)$, $\text{sinc}(\cdot)$, x_t , and x_{t-1} are in $[-1, 1]$. We now demonstrate that the gradient of the ADAA SnakeBeta yields bounded outputs for all inputs. Note that for the sinc function, we have:

$$\frac{d}{dx} \text{sinc}(x) = \begin{cases} 0, & \text{if } x \rightarrow 0 \\ \frac{\cos(x) - \sin(x)}{x}, & \text{otherwise} \end{cases} \quad (15)$$

which, when used to take the partial derivative with respect to x_t and x_{t-1} in Equation 14, brings the following result:

$$\begin{aligned} \frac{\partial y_t}{\partial x_t} &= \frac{1}{2} + \frac{\alpha}{2\beta} \sin(\alpha(x_t + x_{t-1})) \text{sinc}(\alpha(x_t - x_{t-1})) \\ &\quad - \frac{\alpha}{2\beta} \cos(\alpha(x_t + x_{t-1})) \frac{\partial}{\partial x} \text{sinc}(\alpha(x_t - x_{t-1})) \\ \frac{\partial y_t}{\partial x_{t-1}} &= \frac{1}{2} + \frac{\alpha}{2\beta} \sin(\alpha(x_t + x_{t-1})) \text{sinc}(\alpha(x_t - x_{t-1})) \\ &\quad + \frac{\alpha}{2\beta} \cos(\alpha(x_t + x_{t-1})) \frac{\partial}{\partial x} \text{sinc}(\alpha(x_t - x_{t-1})) \end{aligned} \quad (16)$$

where applying the auxiliary angle formula gives the following value range of the two partial derivatives:

$$\frac{\partial y_t}{\partial x_t}, \frac{\partial y_t}{\partial x_{t-1}} \in \left[\frac{\beta - \alpha}{2\beta}, \frac{\beta + \alpha}{2\beta} \right], \quad (17)$$

which is restricted to a reasonable range and avoids the gradient explosion. Following [16, 23], we initialize both α and β to be 1 to guarantee the gradient stability.

B. Anti-Aliased Upsampling Layers

The architecture of the proposed anti-aliased upsampling layer is shown in Figure 2. We replace the ConvTranspose with resampling (zero-interlacing + low-pass filter) to avoid the “tonal artifact” and suppress the aliased components. We apply a channel expansion Conv1D layer with a high-pass filter to convert the zero-interlaced x_0 to a noise-like deterministic prior, which is used to fill the empty high-frequency region of the upsampled signal to improve the training stability (x_0 is the latent representation obtained from the first Conv1D layer in the decoder). The added-up full-band signal is then fed to a channel expansion Conv1D layer to obtain the layer output.

IV. PROPOSED MODELS

In this section, we propose Pupu-Vocoder and Pupu-Codec to facilitate audio generation research, as shown in Figure 4.

A. Model Architecture

As illustrated in Figure 4, Pupu-Codec consists of an encoder, a residual vector quantizer (RVQ) module, a decoder, and four different discriminators. The encoder includes an initial Conv1D layer, five CNN-based Resblocks, and a final Conv1D layer. The RVQ module is adapted from DAC [23]. The decoder includes an initial Conv1D layer, five “AF Conv Blocks”, and a final Conv1D layer. The “AF Conv Blocks” are obtained by modifying the convolution blocks used in BigVGAN [16] and DAC [23] with our proposed anti-aliased activation and upsampling modules. Following [45], we mix both time-domain and TFR-based discriminators to obtain a better synthesis quality, which includes: Multi-Period Discriminator (MPD), Multi-Scale Discriminator (MSD) [17], Multi-Band Discriminator (MBD) [23], and Multi-Scale Sub-Band CQT Discriminator (MS-SB-CQTD) [46]. Replacing the waveform input, encoder, and RVQ module with a mel-spectrogram as the input gives the Pupu-Vocoder model.

B. Training Losses

We adapted the training scheme from DAC [23] to train the Pupu-Codec model, which is illustrated as follows:

$$\begin{aligned} \mathcal{L}_{\text{generator}} &= 15\mathcal{L}_{\text{multi-mel}}(x, \hat{x}) + 0.25\mathcal{L}_{\text{commit}}(z_q, z_e) \\ &+ \mathcal{L}_{\text{code}}(z_e, z_q) + \sum_{m=1}^M [\mathcal{L}_{\text{adv}}(G; D_m) + 2\mathcal{L}_{\text{feat}}(G; D_m)]; \\ \mathcal{L}_{\text{discriminator}} &= \sum_{m=1}^M \mathcal{L}_{\text{adv}}(D_m; G); \end{aligned} \quad (18)$$

where x and \hat{x} are the ground truth and predicted waveform, z_e is the latent representation from encoder, z_q is the quantized z_e reconstructed from discrete tokens, $\mathcal{L}_{\text{code}}$, $\mathcal{L}_{\text{commit}}$, and $\mathcal{L}_{\text{multi-mel}}$ are the codebook, commitment, and multi-scale mel-spectrogram losses, D_m is the m^{th} discriminator, G is the Pupu-Codec model, and \mathcal{L}_{adv} and $\mathcal{L}_{\text{feat}}$ are the adversarial losses and feature matching loss. Removing the codebook and commitment losses gives the training goal of Pupu-Vocoder.

V. EXPERIMENTS

A. Experiment Setup

1) *Datasets*: As suggested by previous works [47–51], we use large-scale data mixtures from different domains to train and evaluate the models for better distinguishability. Specifically, for speech, we use DAPS [52], HQ-TTS [53], AIShell 3 [54], HiFi-TTS [55], HUI-TTS [56], VCTK [57], Bible-TTS [58], EARS [59], and Mana-TTS [60] for training, resulting in 1661.4 hours of multilingual speech; for singing voice, we use NUS-48E [61], Opera [62], VocalSet [63], JSUTSong [64], JaCRC [65], PJS [66], CSD [67], JVS-Music [68], KiSing [69], OpenSinger [70], NHSS [71], PopCS [72], PopBuTFy [73], Opencpop [74], M4Singer [75], SingStyle111 [76], GOAT [77], ACESinger [78], SingNet-SP [79], and an internal dataset for training, resulting in 885.2 hours of multilingual and multi-style singing voice; for music, we use GoodSounds [80], MedleyDB [81], MUSDB18 [82], Slakh2100 [83], Surge Synth [84], Arturia Synth [84], DX7 Synth [84], and MoisesDB [85] for training, resulting in 2343.1 hours of multi-style music tracks; for audio, we use Audioset-Strong [86], BBC Sound Effects ¹, and FreeSound ² for training, resulting in 1811.0 hours audio events. To evaluate the performance of models in different domains, we split the evaluation sets into academic and industrial settings. The academic setting is formed by academic datasets, providing a diverse yet general evaluation, while the industrial setting is formed by a small amount of industrial data, offering a high-quality and professional evaluation. Specifically, for speech, we utilize English, Chinese, Japanese, Korean, French, and German sets from Common Voice [87] as the academic setting. We manually collected voice actor databases from Hitsugi³, ZunzunProject⁴, Voice Seven⁵, Amitaro⁶, Narakuyui⁷, and Matsukane⁸ as the industrial setting; for singing voice, we use GTSinger [88] as the academic setting. We collected Vocaloid databases from Kiritan [89], Namine Ritsu⁹, Voice Seven⁵, Oniku Kurumi¹⁰, Ofutonp¹¹, Yuuri Natsume¹², and Amaboshi Cipher¹³ for industrial setting; for music, we use the Cambridge Mixing Secret¹⁴ database as the academic setting. We utilize an internal music production sample pack database for the industrial setting. For audio, we employ the UrbanSound8K [90], ECE50 [91], and MACS [92] datasets for the academic setting. We utilize an internal sound design sample pack database for industrial settings. Each academic or industrial evaluation set is constructed of 1000 samples that are evenly and randomly extracted from each data source.

¹<https://sound-effects.bbcrewind.co.uk/>

²<https://freesound.org/>

³<https://booth.pm/ja/items/3382115>

⁴<https://zunko.jp/>

⁵<https://voiceseven.com/>

⁶<http://amitaro.net/>

⁷<https://narakuyui.fanbox.cc/posts/7082575>

⁸https://x.com/mochi_jin_voice

⁹<https://www.canon-voice.com/>

¹⁰<https://onikuru.info/>

¹¹<https://sites.google.com/view/oftn-utagoedb/>

¹²<https://ksdcm1ng.wixsite.com/njksofficial>

¹³<https://parapluie2c56m.wixsite.com/mysite>

¹⁴<https://www.cambridge-mt.com/ms3/mtk>

TABLE I: Statistics of the test signal benchmark.

Type	F0 Range	Dur. (min)	Samp. Rate (Hz)
Sine	[261.63 Hz, 3951.04 Hz]	6	44.1k
Sawtooth	[261.63 Hz, 3951.04 Hz]	6	44.1k
Triangle	[261.63 Hz, 3951.04 Hz]	6	44.1k

We additionally constructed a test signal benchmark to show the effectiveness of the anti-aliased modules following [93]. In particular, we use three different test signal types, including the sine, sawtooth, and triangle wave signals. Table I illustrates the construction details. We use Serum¹⁵ to generate the test signals to utilize its outstanding anti-aliasing ability. We use Reaper¹⁶ and Reascript¹⁷ for automatic command-line audio generation. For each signal, we generate 10-second MIDI notes from C4 (261.63 Hz) to B7 (3951.04 Hz), which will then be symmetrically trimmed at the beginning and end to eliminate the clicks caused by the attack and release phases in the attack-decay-sustain-release (ADSR) generation process, resulting in 48 5-second segments.

2) *Preprocessing*: We process the training and evaluation datasets to 44.1 kHz mono WAV files. For extracting the mel-spectrograms, we use an FFT size of 2048, a hop size of 512, a window length of 2048, and 128 mel filters, which are further normalized in log-scale with values $\leq 1e-5$ clipped to 0.

3) *Configurations*: The Pupu-Codec is modified from DAC [23]. Based on the official repository¹⁸, we change the encoder channel dimension to 32 for the small model and to 48 for the large model. We change the encoder and decoder ratios to [2, 2, 2, 8, 8], and encoder and decoder kernel sizes to [4, 4, 4, 16, 16], and leave the RVQ module unmodified to have a frame rate of 86 Hz and a maximum bitrate of 8 kbps. The Pupu-Vocoder is modified from BigVGAN [16]. Based on the official repository¹⁹, we modify the upsampling ratios to [8, 8, 2, 2, 2], upsampling kernel sizes to [16, 16, 4, 4, 4], and leave the initial channel size unmodified. For the anti-aliased activation and upsampling modules, we apply ADAA with an oversampling factor of 2 for the activation function. For the upsampling layer, we use a kernel size of 7, a stride of 1, and a padding of 1 for the noise convolution, and a kernel size of 1, a stride of 1, and a padding of 1 for the channel expansion convolution. For the discriminators, we use periods of [2, 3, 5, 7, 11, 17, 23, 37] for the MPD. We compute 10 octaves and change the hop sizes to [1024, 512, 512] for the MS-SB-CQTD, while leaving the MSD and MBD unmodified.

4) *Baselines*: We use various baselines to illustrate the effectiveness of our proposed models. We use HiFi-GAN [17] and BigVGAN [16] as neural vocoder baselines and use Encoddec [22], DAC [23], and BigCodec [94] as neural codec baselines. We additionally use Vocos [33] as the aliasing-free TF-domain referential system. We maintain all the codec systems at the same frame rate and maximum bitrate for a fair comparison by adjusting their encoder and decoder ratios.

¹⁵<https://xferrecords.com/products/serum-2>

¹⁶<https://www.reaper.fm/>

¹⁷<https://www.reaper.fm/sdk/reascript/reascript.php>

¹⁸<https://github.com/descriptinc/descript-audio-codec>

¹⁹<https://github.com/NVIDIA/BigVGAN>

The detailed model configurations are illustrated as follows:

- **HiFi-GAN** - We implement the HiFi-GAN model using²⁰ and modify the upsampling ratios to [8, 8, 2, 2, 2], upsampling kernel sizes to [16, 16, 4, 4, 4], and the initial channel size to 512 based on the V1 model.
- **BigVGAN** - We implement the BigVGAN using¹⁹. We modify the upsampling ratios to [8, 8, 2, 2, 2] and the upsampling kernel sizes to [16, 16, 4, 4, 4] for the small model, while keeping the large model unchanged.
- **Encoddec** - We implement the Encoddec model using an open-source reproduction²¹ and modify the encoder and decoder ratios to [2, 2, 2, 8, 8], encoder and decoder kernel sizes to [4, 4, 4, 16, 16], and target bandwidths to be [1.78 kbps, 2.67 kbps, 5.33 kbps, 8 kbps].
- **DAC** - We implement the DAC using¹⁸ and modify the encoder and decoder ratios to [2, 2, 2, 8, 8], and encoder and decoder kernel sizes to [4, 4, 4, 16, 16].
- **BigCodec** - We implement the BigCodec using²² and modify the encoder and decoder ratios to [2, 2, 2, 2, 4, 8], encoder and decoder kernel sizes to [4, 4, 4, 4, 8, 16], codebook size to 1024, and codebook number to 9.
- **Vocos** - We implement the Vocos model using²³ and modify the upsampling ratios to [8, 8, 2, 2, 2], and upsampling kernel sizes to [16, 16, 4, 4, 4].

5) *Training*: All the models are trained using the AdamW optimizer with $\beta_1 = 0.8$ and $\beta_2 = 0.99$, a learning rate of 1e-4, and an exponential decay scheduler with a factor $\gamma = 0.999996$. All the experiments are conducted on 8 H200 GPUs with the maximum available batch size for 1M steps.

B. Evaluation Metrics

1) *Objective Evaluation*: We use the Amphion [95] toolkit for objective evaluation. For the test signal benchmark, we use the aliasing-to-harmonic ratio (AHR) following [93] (with matching definition to the original aliasing-to-signal ratio, but avoiding abbreviation clash with ASR). For the speech and singing voice, we use the predictive mean opinion score (MOS-Pred), F0 root mean square error (FORMSE), and periodicity (Periodicity) following [96]. We use the Sheet [97] toolkit to predict the MOS value. For music and audio, we use the Fréchet audio distance (FAD) [98, 99], multi-scale STFT distance (M-STFT), and VisQOL [100] following DAC [23].

2) *Subjective Evaluation*: We conduct MUSHRA [101] and Comparative Mean Opinion Score (C-MOS) tests for the subjective evaluation. For MUSHRA, 4 samples per domain are assessed. Listeners are asked to assign quality scores between 1 and 100 for different systems. We use the ground-truth audio as the reference and its 16 kHz low-pass filtered version as the hidden anchor. For C-MOS, 6 samples are evaluated. Listeners are asked to assign quality scores on a scale of -3 to 3 compared to the baseline. We invite 20 volunteers who are experienced in audio generation to attend the evaluation. All tests are conducted online, and listeners are instructed to use headphones in a quiet environment.

²⁰<https://github.com/jik876/hifi-gan>

²¹<https://github.com/ZhikangNiu/encoddec-pytorch>

²²<https://github.com/Aria-K-Alethia/BigCodec>

²³<https://github.com/gemelo-ai/vocos>

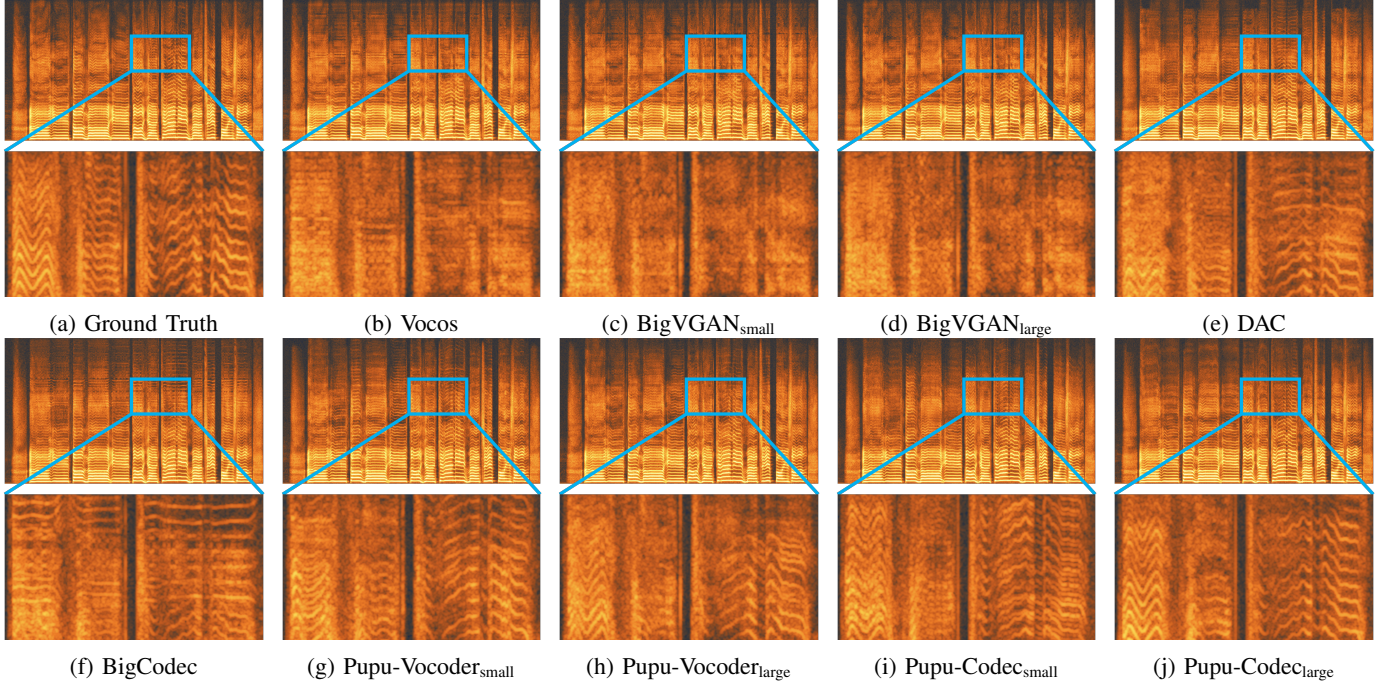


Fig. 5: Spectrogram visualization with a zoomed-in view of high-frequency harmonic components (around 16 kHz) regarding a representative singing voice example copy-synthesized by different neural vocoder and codec models.

TABLE II: AHR results of different activation and upsampling modules on the test signal benchmark. The values are reported in dB scale. The best and the second best results of every column in each baseline setting are **bold** and underlined.

Module	AHR (↓)			
	Sine	Sawtooth	Triangle	Average
LeakyReLU	-17.68	-36.70	-21.39	-25.25
ELU	<u>-39.76</u>	<u>-55.40</u>	-39.20	<u>-44.79</u>
SnakeBeta	-38.32	-50.37	-30.19	-39.63
Ours	-42.05	-58.33	<u>-37.47</u>	-45.95
ConvTranspose	-24.28	-16.11	-24.62	-21.67
Linear Interpolation	-63.48	<u>-29.14</u>	<u>-51.71</u>	<u>-48.11</u>
Nearest Interpolation	-34.20	-14.83	-28.54	-25.86
Ours	<u>-62.87</u>	-39.92	-59.00	-53.93

C. Experimental Results

1) *Effectiveness of the Anti-Aliased Modules*: The objective evaluation results on the test signal benchmark are shown in Table II. For the activation function, the widely used LeakyReLU, popularized by HiFi-GAN [17], introduced the most aliasing artifacts, followed by the now commonly used SnakeBeta. In contrast, ELU reduced aliasing artifacts by smoothing the sharp nonlinearity of ReLU with an exponential transition, but still performed slightly worse than our proposed ADAA SnakeBeta. For the upsampling layer, the randomly initialized ConvTranspose obtained the worst performance, introducing both the “mirrored” aliasing artifacts and “tonal artifact”. Although the linear and nearest interpolations can mitigate this issue to some extent, their effectiveness remains limited, since they introduce additional “filter artifact” due to their poor filter designs, as we discussed in Section II.

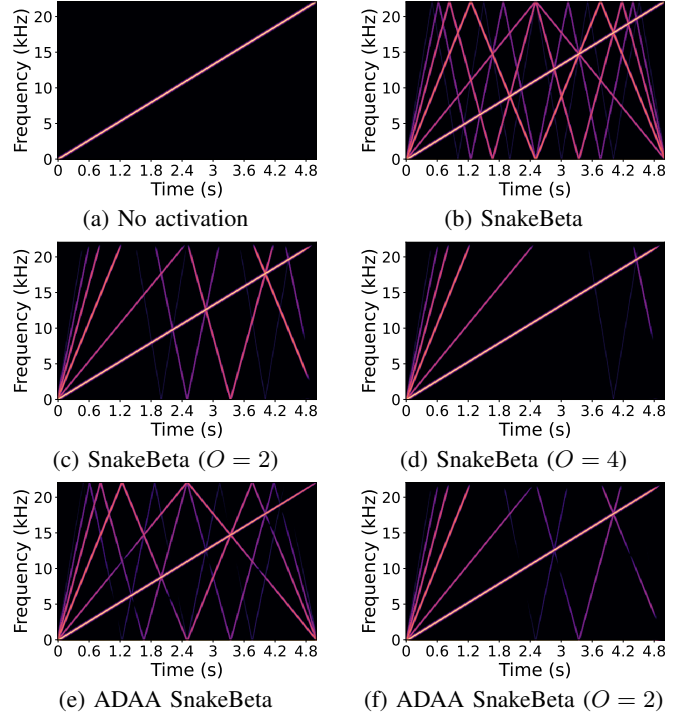


Fig. 6: Anti-aliasing case study by passing a sine sweep through different activation functions. “O” is the oversampling factor.

To better illustrate the effectiveness of the proposed ADAA SnakeBeta, we further conducted a case study by passing a sine sweep through different activation functions with various oversampling factors, as shown in Figure 6. It can be observed that our ADAA SnakeBeta with only 2× oversampling can achieve a similar level of aliasing suppression compared with SnakeBeta with 4× oversampling, confirming its effectiveness.

TABLE III: Analysis-synthesis results of different systems on speech and singing voice. The best and the second best results of every column (except those from Ground Truth) in each domain and baseline setting are **bold** and underlined. “Acad.” means academic setting and “Ind.” means industrial setting. The MUSHRA scores are within 95% Confidence Interval (CI).

Domain	System	# Param	Mos-Pred (\uparrow)		FORMSE (\downarrow)		Periodicity (\downarrow)		MUSHRA (\uparrow)	
			Acad.	Ind.	Acad.	Ind.	Acad.	Ind.	Acad.	Ind.
Speech	Ground Truth	/	3.77	4.29	0.00	0.00	0.0000	0.0000	89.13 ± 0.77	89.49 ± 0.70
	Vocos	14M	3.22	4.08	68.67	40.09	0.0291	0.0084	58.94 ± 1.60	69.22 ± 1.41
	HiFi-GAN	14M	3.29	4.11	80.40	46.64	0.0296	0.0087	55.56 ± 1.57	67.73 ± 1.34
	BigVGAN _{small}	14M	3.39	4.08	61.35	40.96	0.0296	0.0115	61.13 ± 1.64	70.27 ± 1.23
	BigVGAN _{large}	122M	3.47	4.14	<u>50.30</u>	<u>33.93</u>	0.0246	0.0074	67.53 ± 1.46	73.22 ± 1.20
	Pupu-Vocoder _{small}	14M	<u>3.49</u>	<u>4.23</u>	58.25	37.28	<u>0.0272</u>	<u>0.0080</u>	70.97 ± 1.54	75.97 ± 1.24
	Pupu-Vocoder _{large}	122M	3.53	4.26	48.88	32.01	0.0290	0.0099	73.06 ± 1.57	80.05 ± 1.14
	EnCodec	59M	3.47	4.25	49.60	29.96	0.0206	0.0080	66.84 ± 1.64	73.51 ± 1.29
	DAC	154M	3.60	4.29	32.93	24.46	0.0128	0.0044	79.72 ± 1.36	87.24 ± 0.68
	BigCodec	412M	3.65	<u>4.28</u>	35.27	23.73	0.0148	0.0043	82.06 ± 1.30	87.32 ± 0.66
Singing Voice	Pupu-Codec _{small}	32M	3.54	4.25	38.83	<u>23.47</u>	<u>0.0116</u>	0.0037	76.53 ± 1.48	78.68 ± 1.18
	Pupu-Codec _{large}	119M	<u>3.61</u>	4.29	<u>35.15</u>	22.32	0.0111	0.0040	81.63 ± 1.24	86.14 ± 0.71
	Ground Truth	/	4.18	4.33	0.00	0.00	0.0000	0.0000	86.13 ± 0.82	89.30 ± 0.74
	Vocos	14M	3.66	3.61	32.56	25.22	0.0933	0.1112	49.84 ± 1.38	42.92 ± 1.23
	HiFi-GAN	14M	3.84	3.93	32.67	22.59	0.0962	0.1211	56.29 ± 1.17	57.68 ± 1.09
	BigVGAN _{small}	14M	3.76	3.78	32.07	21.34	0.0949	0.1159	51.26 ± 1.24	49.19 ± 1.19
	BigVGAN _{large}	122M	3.88	3.92	<u>26.56</u>	<u>17.92</u>	0.0754	0.0912	58.28 ± 1.26	53.08 ± 1.14
	Pupu-Vocoder _{small}	14M	<u>4.08</u>	<u>4.22</u>	29.17	19.13	0.0839	0.1110	68.26 ± 1.20	65.73 ± 1.25
	Pupu-Vocoder _{large}	122M	4.09	4.24	25.86	17.12	<u>0.0827</u>	<u>0.1011</u>	70.05 ± 1.14	70.84 ± 1.15
	EnCodec	59M	3.97	4.19	26.72	15.76	0.0875	0.1349	54.74 ± 1.41	57.16 ± 1.26
Music	DAC	154M	<u>4.16</u>	4.33	19.57	12.38	<u>0.0557</u>	0.0904	80.55 ± 0.99	85.43 ± 0.85
	BigCodec	412M	4.17	<u>4.32</u>	20.44	<u>12.37</u>	0.0598	0.0860	82.74 ± 0.84	84.81 ± 0.83
	Pupu-Codec _{small}	32M	4.10	<u>4.31</u>	22.31	13.70	0.0559	0.0979	75.61 ± 1.28	78.97 ± 1.16
	Pupu-Codec _{large}	119M	4.17	4.33	<u>19.84</u>	12.34	0.0528	0.0834	83.79 ± 0.94	85.65 ± 0.86

2) *Effectiveness on Speech, Singing, Music, and Audio:* We run experiments on speech, singing voice, music, and audio to show the effectiveness of our proposed models. The evaluation results are illustrated in Table III and Table IV. For speech, regarding neural vocoders, both Pupu-Vocoder models have better scores on MOS-Pred and FORMSE. While they obtain slightly lower performance in Periodicity, their MUSHRA scores consistently outperform all baselines, confirming their effectiveness; for neural codecs, Pupu-Codec_{small} outperforms EnCodec and achieves performance on par with significantly larger models, showing its parameter efficiency. Meanwhile, Pupu-Codec_{large} shows comparable performance to baselines across both objective and subjective metrics, validating its effectiveness. For singing voice, a similar conclusion can be drawn from Pupu-Vocoder models and Pupu-Codec_{small} as in speech. For Pupu-Codec_{large}, although it yields comparable objective results to the baselines, subjective evaluation reveals its superior performance, confirming the effectiveness of the anti-aliased modules. For music and audio, regarding neural vocoders, Pupu-Vocoder_{small} performs on par with HiFi-GAN and BigVGAN_{small}, and Pupu-Vocoder_{large} yields comparable FAD and VisQOL with better M-STFT scores, while having significantly better performance on MUSHRA, illustrating its effectiveness; regarding neural codecs, the Pupu-Codec_{small}

model outperforms EnCodec and achieves performance on par with other baselines, while Pupu-Codec_{large} consistently outperform all the baseline systems both objectively and subjectively, showing its superior synthesis quality.

We further conducted a case study on singing voice to illustrate the effectiveness of our proposed models, as shown in the Figure 5. As we can see, the Vocos and BigGAN models are unable to generate reasonable harmonic structures at such a high frequency, instead producing noise. In contrast, the DAC and BigCodec models can generate harmonic components in high-frequency bands but also introduce a significant amount of aliased components, resulting in blurred and noisy high-frequency parts that degrade the synthesis quality. Unlike these baseline models, our proposed models can produce harmonics in high-frequency bands without introducing aliasing artifacts. Comparing our internal variants, the Pupu-Vocoder models tend to generate harmonic components with distorted shapes, which may be due to their lack of implicit phase modeling. The Pupu-Codec_{small} model can generate harmonic components with the correct shape but tends to overly produce harmonics that do not appear in the original waveform, resulting in hissing noises in the background. In contrast, the Pupu-Codec_{large} model can accurately reconstruct the full harmonic structure, benefiting from its increased model capacity.

TABLE IV: Analysis-synthesis results of different systems on music and audio. The best and the second best results of every column (except those from Ground Truth) in each domain and baseline setting are **bold** and underlined. “Acad.” means academic setting and “Ind.” means industrial setting. The MUSHRA scores are within 95% Confidence Interval (CI).

Domain	System	# Param	FAD (↓)		M-STFT (↓)		ViSQOL (↑)		MUSHRA (↑)	
			Acad.	Ind.	Acad.	Ind.	Acad.	Ind.	Acad.	Ind.
Music	Ground Truth	/	0.000	0.000	0.00	0.00	5.00	5.00	87.24 ± 0.85	86.48 ± 1.26
	Vocos	14M	0.017	0.037	0.72	0.83	4.54	4.42	58.89 ± 1.42	48.00 ± 1.69
	HiFi-GAN	14M	0.044	0.085	0.83	0.90	4.33	4.32	54.84 ± 1.28	37.74 ± 1.57
	BigVGAN _{small}	14M	0.021	0.054	0.79	<u>0.88</u>	4.55	4.46	58.43 ± 1.17	42.55 ± 1.60
	BigVGAN _{large}	122M	0.014	0.044	0.82	0.93	4.61	4.54	65.68 ± 1.34	50.42 ± 1.90
	Pupu-Vocoder _{small}	14M	0.043	0.087	<u>0.75</u>	0.91	4.37	4.35	56.35 ± 1.43	42.87 ± 1.90
	Pupu-Vocoder _{large}	122M	<u>0.017</u>	<u>0.049</u>	0.71	0.83	<u>4.60</u>	<u>4.48</u>	70.38 ± 1.26	56.42 ± 1.66
	EnCodec	59M	0.141	0.136	0.88	0.95	4.05	4.23	52.65 ± 2.53	39.97 ± 1.79
	DAC	154M	0.040	0.045	<u>0.76</u>	0.83	4.31	<u>4.43</u>	71.78 ± 1.24	72.65 ± 1.50
	BigCodec	412M	<u>0.033</u>	0.029	0.86	<u>0.88</u>	<u>4.32</u>	4.44	72.87 ± 1.18	73.09 ± 1.25
Audio	Pupu-Codec _{small}	32M	0.036	0.066	0.78	0.90	4.12	4.29	68.16 ± 1.40	65.23 ± 1.60
	Pupu-Codec _{large}	119M	0.019	<u>0.033</u>	0.75	0.83	4.34	4.44	73.14 ± 1.27	74.39 ± 1.40
	Ground Truth	/	0.000	0.000	0.00	0.00	5.00	5.00	88.22 ± 0.95	82.83 ± 1.02
	Vocos	14M	0.022	0.018	0.88	0.84	4.50	4.55	74.50 ± 1.30	64.25 ± 1.37
	HiFi-GAN	14M	0.048	0.037	0.88	0.95	4.23	4.38	63.59 ± 1.53	58.78 ± 1.52
	BigVGAN _{small}	14M	0.019	0.020	<u>0.84</u>	0.91	4.46	4.56	71.97 ± 1.45	66.11 ± 1.50
	BigVGAN _{large}	122M	0.013	0.017	0.97	0.95	4.53	4.61	76.66 ± 1.35	73.17 ± 1.41
	Pupu-Vocoder _{small}	14M	0.031	0.032	0.88	<u>0.90</u>	4.24	4.39	71.47 ± 1.43	65.28 ± 1.50
	Pupu-Vocoder _{large}	122M	<u>0.017</u>	<u>0.018</u>	0.83	0.86	<u>4.47</u>	<u>4.58</u>	77.84 ± 1.22	73.47 ± 1.23
	EnCodec	59M	0.207	0.089	1.08	1.07	3.91	3.96	55.56 ± 1.54	45.36 ± 1.50
Audio	DAC	154M	0.087	0.049	0.91	<u>0.92</u>	4.14	4.25	74.56 ± 1.51	70.56 ± 1.18
	BigCodec	412M	0.079	<u>0.042</u>	1.03	0.99	<u>4.18</u>	<u>4.27</u>	<u>75.00 ± 1.28</u>	<u>73.75 ± 1.08</u>
	Pupu-Codec _{small}	32M	<u>0.072</u>	0.060	<u>0.90</u>	0.93	3.98	4.02	69.28 ± 1.56	67.86 ± 1.37
	Pupu-Codec _{large}	119M	0.046	0.039	0.88	0.90	4.19	4.29	75.59 ± 1.36	75.00 ± 1.09

3) *Effectiveness on Dynamic Bitrate Encoding*: We also explored the performance of our proposed Pupu-Codec models under the dynamic bitrate encoding scenario, as illustrated in Figure V. We perform our evaluation in the industrial singing voice setting, as its rich harmonic structure and higher modeling difficulty make it easier to distinguish the quality of different models. Specifically, while the EnCodec model exhibits severe quality degradation in low-bitrate conditions, our proposed Pupu-Codec_{small} model maintains performance and is comparable to the DAC and BigCodec models, despite having fewer parameters. Meanwhile, our Pupu-Codec_{large} model exhibits comparable objective metrics to those of DAC and BigCodec models. Moreover, in subjective evaluation, it outperforms the DAC and BigCodec models in high and medium-bitrate scenarios (8 kbps, 5.33 kbps, and 2.67 kbps) and is on par with them in low-bitrate scenarios (1.78 kbps). We hypothesize that this convergence occurs because, at such restricted bitrates, the information bottleneck limits the reconstruction of high-frequency components, for which our approach is particularly effective. Nevertheless, despite this challenge, our proposed Pupu-Codec models still achieve remarkable performance compared to the baseline models.

4) *Ablation Study*: We conducted an ablation study on singing voice to illustrate the effectiveness of our proposed anti-aliased modules, as shown in Table VI. For activation functions, oversampling is crucial for audio quality; removing it degrades synthesis quality both objectively and subjectively. Meanwhile, their anti-aliasing abilities also correlate with the synthesis quality. Among them, our ADAA SnakeBeta achieves the best result both objectively and subjectively, followed by the SnakeBeta and ELU. For different upsampling layers, the ConvTranspose, linear, and nearest interpolation achieve similar results objectively. The linear and nearest interpolation methods achieve the best subjective performance, as they do not exhibit “tonal artifacts” and attenuate part of the “mirrored” aliasing artifacts compared to the ConvTranspose layer. Finally, the deterministic noise prior proves to be a crucial factor in achieving synthesis fidelity; removing it would greatly degrade the synthesis performance both objectively and subjectively. This aligns with previous work [102], which demonstrates that standard neural networks exhibit spectral bias, hindering their ability to reconstruct high-frequency details. This issue can be resolved by projecting inputs into a high-frequency prior, thus overcoming the low-frequency bias.

TABLE V: Analysis-synthesis results of different systems on singing voice in different bitrates. The best and the second best results of every column in each domain and bitrate setting are **bold** and underlined. “Acad.” means academic setting and “Ind.” means industrial setting. The MUSHRA scores are within 95% Confidence Interval (CI).

Bitrate	System	# Param	Mos-Pred (\uparrow)		FORMSE (\downarrow)		Periodicity (\downarrow)		MUSHRA (\uparrow)
			Acad.	Ind.	Acad.	Ind.	Acad.	Ind.	
/	Ground Truth	/	4.18	4.33	0.00	0.00	0.0000	0.0000	86.78 \pm 0.23
8 kbps	EnCodec	59M	3.97	4.19	26.72	15.76	0.0875	0.1349	56.81 \pm 1.59
	DAC	154M	4.16	4.33	19.57	12.38	<u>0.0557</u>	0.0904	<u>81.39</u> \pm 1.07
	BigCodec	412M	4.17	<u>4.32</u>	20.44	<u>12.37</u>	0.0598	<u>0.0860</u>	<u>81.14</u> \pm 1.16
	Pupu-Codec _{small}	32M	4.10	4.31	22.31	13.70	0.0559	0.0979	72.97 \pm 1.38
	Pupu-Codec _{large}	119M	4.17	4.33	<u>19.84</u>	12.34	0.0528	0.0834	82.64 \pm 1.09
5.33 kbps	EnCodec	59M	3.82	4.08	30.79	18.04	0.0993	0.1417	52.61 \pm 1.44
	DAC	154M	4.15	4.32	21.50	13.84	<u>0.0630</u>	<u>0.0974</u>	<u>79.22</u> \pm 1.09
	BigCodec	412M	<u>4.14</u>	<u>4.30</u>	24.05	14.65	0.0719	0.1008	74.25 \pm 1.13
	Pupu-Codec _{small}	32M	4.05	4.28	25.52	16.64	0.0667	0.1063	73.92 \pm 1.37
	Pupu-Codec _{large}	119M	4.15	4.32	<u>23.53</u>	<u>14.38</u>	0.0624	0.0941	81.56 \pm 0.87
2.67 kbps	EnCodec	59M	3.34	3.64	44.99	26.10	0.1410	0.1673	42.57 \pm 1.36
	DAC	154M	4.06	4.27	27.05	18.24	0.0825	0.1182	<u>72.68</u> \pm 0.97
	BigCodec	412M	<u>4.02</u>	4.23	30.37	20.19	0.0930	0.1250	<u>70.43</u> \pm 1.29
	Pupu-Codec _{small}	32M	3.87	4.17	32.64	21.87	0.0901	0.1279	67.51 \pm 1.39
	Pupu-Codec _{large}	119M	4.06	<u>4.25</u>	<u>29.84</u>	<u>19.48</u>	<u>0.0841</u>	<u>0.1195</u>	73.97 \pm 1.22
1.78 kbps	EnCodec	59M	2.64	2.84	64.44	51.13	0.1967	0.2277	25.94 \pm 1.22
	DAC	154M	3.94	4.18	33.34	22.53	0.1005	0.1343	67.53 \pm 1.21
	BigCodec	412M	3.84	4.08	36.35	25.76	0.1051	0.1437	55.00 \pm 1.28
	Pupu-Codec _{small}	32M	3.65	3.95	39.16	28.31	0.1133	0.1521	53.33 \pm 1.29
	Pupu-Codec _{large}	119M	<u>3.87</u>	<u>4.11</u>	<u>35.51</u>	<u>23.61</u>	<u>0.1018</u>	<u>0.1365</u>	<u>65.17</u> \pm <u>1.18</u>

TABLE VI: Ablation experiment results on singing voice. The best and the second best results of every column in each ablation setting are **bold** and underlined. “Acad.” means academic setting, “Ind.” means industrial setting, “w/o” means “without”, and “ \rightarrow ” means “replace”. The C-MOS scores are within 95% Confidence Interval (CI).

System	Mos-Pred (\uparrow)		FORMSE (\downarrow)		Periodicity (\downarrow)		C-MOS (\uparrow)
	Acad.	Ind.	Acad.	Ind.	Acad.	Ind.	
Pupu-Vocoder _{small}	4.081	4.221	29.17	19.13	0.0839	0.1110	/
w/o Oversampling	3.991	4.133	33.40	27.04	0.0988	0.1351	-0.38 \pm 0.02
Ours \rightarrow LeakyReLU	3.839	3.940	34.83	26.82	0.1060	0.1452	-1.45 \pm 0.02
Ours \rightarrow ELU	3.972	4.075	34.85	23.85	0.1019	<u>0.1297</u>	-0.93 \pm 0.02
Ours \rightarrow SnakeBeta	<u>4.047</u>	<u>4.153</u>	<u>30.97</u>	<u>20.11</u>	<u>0.0934</u>	<u>0.1360</u>	-0.52 \pm 0.02
w/o Deterministic Prior	3.811	3.896	35.35	28.14	0.1059	0.1488	-1.49 \pm 0.02
Ours \rightarrow ConvTranspose	4.040	4.182	29.35	20.76	0.0871	<u>0.1141</u>	-0.15 \pm 0.02
Ours \rightarrow Linear Interpolation	4.042	<u>4.186</u>	<u>29.21</u>	<u>19.67</u>	0.0883	0.1178	-0.01 \pm 0.02
Ours \rightarrow Nearest Interpolation	<u>4.044</u>	4.170	29.61	19.82	<u>0.0843</u>	0.1148	-0.04 \pm 0.02

VI. CONCLUSION

This paper addresses the synthesis fidelity limitations in upsampling-based neural audio generation that are introduced by inadequately designed model architectures. By analyzing and identifying the sources of “folded-back” and “mirrored” aliasing artifacts, as well as the “tonal artifact”, we propose Pupu-Vocoder and Pupu-Codec, which incorporate our novel anti-aliased activation and upsampling modules. Experimental results demonstrate that our proposed models can consistently outperform existing baselines across singing voice, music, and audio, while yielding comparable results on speech.

VII. ACKNOWLEDGMENT

This work is a joint effort by Spellbrush, Aalto University, and The Chinese University of Hong Kong, Shenzhen. We acknowledge the Aalto Science-IT project for computational resources and the EuroHPC Joint Undertaking for awarding this project access to the EuroHPC supercomputer LUMI, hosted by CSC (Finland) and the LUMI consortium. Finally, the first author would like to acknowledge her partner, Zeyu Dou, for his consistent support throughout her life and career. In recognition of his fondness for rabbits, *Pupu* (‘bunny’ in Finnish) was adopted as the prefix for the proposed models.

REFERENCES

[1] Y. Wang *et al.*, “MaskGCT: Zero-Shot Text-to-Speech with Masked Generative Codec Transformer,” in *Proc. ICLR*, 2025.

[2] X. Zhang *et al.*, “Vevo: Controllable Zero-Shot Voice Imitation with Self-Supervised Disentanglement,” in *Proc. ICLR*, 2025.

[3] C. Wang *et al.*, “Neural Codec Language Models are Zero-Shot Text to Speech Synthesizers,” *arXiv:2301.02111*, 2023.

[4] N. Kalchbrenner *et al.*, “Efficient Neural Audio Synthesis,” in *Proc. ICML*, 2018, pp. 2415–2424.

[5] J. Valin and J. Skoglund, “LPCNet: Improving Neural Speech Synthesis through Linear Prediction,” in *Proc. Int. Conf. Acoust. Speech Signal Process.*, 2019, pp. 5891–5895.

[6] A. van den Oord *et al.*, “WaveNet: A Generative Model for Raw Audio,” in *Proc. ISCA Workshop Speech Synth.*, 2016, p. 125.

[7] T. Luo, X. Miao, and W. Duan, “WaveFM: A High-Fidelity and Efficient Vocoder Based on Flow Matching,” in *Proc. ACL*, 2025, pp. 2187–2198.

[8] W. Ping, K. Peng, K. Zhao, and Z. Song, “WaveFlow: A Compact Flow-based Model for Raw Audio,” in *Proc. ICML*, vol. 119, 2020, pp. 7706–7716.

[9] R. Prenger, R. Valle, and B. Catanzaro, “Waveglow: A Flow-based Generative Network for Speech Synthesis,” in *Proc. Int. Conf. Acoust. Speech Signal Process.*, 2019, pp. 3617–3621.

[10] N. Chen, Y. Zhang, H. Zen, R. J. Weiss, M. Norouzi, and W. Chan, “WaveGrad: Estimating Gradients for Waveform Generation,” in *Proc. ICLR*, 2021.

[11] Z. Kong, W. Ping, J. Huang, K. Zhao, and B. Catanzaro, “DiffWave: A Versatile Diffusion Model for Audio Synthesis,” in *Proc. ICLR*, 2021.

[12] T. D. Nguyen, J.-H. Kim, Y. Jang, J. Kim, and J. S. Chung, “Fregrad: Lightweight and Fast Frequency-Aware Diffusion Vocoder,” in *Proc. Int. Conf. Acoust. Speech Signal Process.*, 2024, pp. 10736–10740.

[13] P. Agrawal, T. Köhler, Z. Xiu, P. Serai, and Q. He, “Ultra-Lightweight Neural Differential DSP Vocoder for High Quality Speech Synthesis,” in *Proc. Int. Conf. Acoust. Speech Signal Process.*, 2024, pp. 10066–10070.

[14] L. Juvela, B. Bollepalli, V. Tsiaras, and P. Alku, “GlotNet - A Raw Waveform Model for the Glottal Excitation in Statistical Parametric Speech Synthesis,” *IEEE/ACM Trans. Audio Speech Lang. Process.*, vol. 27, pp. 1019–1030, 2019.

[15] D. Wu *et al.*, “DDSP-based Singing Vocoders: A New Subtractive-based Synthesizer and A Comprehensive Evaluation,” in *Proc. ISMIR*, 2022, pp. 76–83.

[16] S. Lee, W. Ping, B. Ginsburg, B. Catanzaro, and S. Yoon, “BigVGAN: A Universal Neural Vocoder with Large-Scale Training,” in *Proc. ICLR*, 2023.

[17] J. Su, Z. Jin, and A. Finkelstein, “HiFi-GAN: High-Fidelity Denoising and Dereverberation Based on Speech Deep Features in Adversarial Networks,” in *Proc. Interspeech*, 2020, pp. 4506–4510.

[18] S. Liao, S. Lan, and A. G. Zachariah, “EVA-GAN: Enhanced Various Audio Generation via Scalable Generative Adversarial Networks,” *arXiv:2402.00892*, 2024.

[19] J. L. Flanagan and R. M. Golden, “Phase Vocoder,” *Bell system technical Journal*, vol. 45, pp. 1493–1509, 1966.

[20] H. Kawahara, “STRAIGHT, exploitation of the other aspect of VOCODER: Perceptually isomorphic decomposition of speech sounds,” *Acoust. Sci. Technol.*, vol. 27, pp. 349–353, 2006.

[21] M. Morise, F. Yokomori, and K. Ozawa, “WORLD: A Vocoder-Based High-Quality Speech Synthesis System for Real-Time Applications,” *IEICE Trans. Inf. Syst.*, vol. 99, pp. 1877–1884, 2016.

[22] A. Défossez, J. Copet, G. Synnaeve, and Y. Adi, “High Fidelity Neural Audio Compression,” *Trans. Mach. Learn. Res.*, vol. 2023, 2023.

[23] R. Kumar, P. Seetharaman, A. Luebs, I. Kumar, and K. Kumar, “High-Fidelity Audio Compression with Improved RVQGAN,” in *Proc. NeurIPS*, 2023.

[24] X. Zhang, D. Zhang, S. Li, Y. Zhou, and X. Qiu, “SpeechTokenizer: Unified Speech Tokenizer for Speech Large Language Models,” *Proc. ICLR*, 2023.

[25] F. Mentzer, D. Minnen, E. Agustsson, and M. Tschannen, “Finite Scalar Quantization: VQ-VAE Made Simple,” in *Proc. ICLR*, 2024.

[26] A. Van Den Oord, O. Vinyals, and K. Kavukcuoglu, “Neural Discrete Representation Learning,” *Proc. NeurIPS*, 2017.

[27] N. Zeghidour, A. Luebs, A. Omran, J. Skoglund, and M. Tagliasacchi, “SoundStream: An End-to-End Neural Audio Codec,” *IEEE/ACM Trans. Audio Speech Lang. Process.*, vol. 30, pp. 495–507, 2022.

[28] D. Afchar, G. Meseguer-Brocal, K. Akesbi, and R. Hennequin, “A Fourier Explanation of AI-music Artifacts,” in *Proc. ISMIR*, 2025.

[29] J. Pons, S. Pascual, G. Cengarle, and J. Serrà, “Upsampling Artifacts in Neural Audio Synthesis,” in *Proc. Int. Conf. Acoust. Speech Signal Process.*, 2021, pp. 3005–3009.

[30] Z. Shang, H. Zhang, P. Zhang, L. Wang, and T. Li, “Analysis and Solution to Aliasing Artifacts in Neural Waveform Generation Models,” *Applied Acoustics*, vol. 203, p. 109183, 2023.

[31] R. Yoneyama, A. Miyashita, R. Yamamoto, and T. Toda, “Wavehax: Aliasing-Free Neural Waveform Synthesis Based on 2D Convolution and Harmonic Prior for Reliable Complex Spectrogram Estimation,” *IEEE/ACM Trans. Audio Speech Lang. Process.*, vol. 33, 2025.

[32] T. Feng *et al.*, “STFTCodec: High-Fidelity Audio Compression through Time-Frequency Domain Representation,” in *Proc. IEEE Int. Conf. Multimed. Expo*, 2025.

[33] H. Siuzdak, “Vocos: Closing the gap between time-domain and Fourier-based neural vocoders for high-quality audio synthesis,” in *Proc. ICLR*, 2024.

[34] S. Bilbao, F. Esqueda, J. D. Parker, and V. Välimäki, “Antiderivative Antialiasing for Memoryless Nonlinear-

ities,” *IEEE Signal Process. Lett.*, vol. 24, pp. 1049–1053, 2017.

[35] J. D. Parker, V. Zavalishin, and E. Le Bivic, “Reducing the Aliasing of Nonlinear Waveshaping using Continuous-Time Convolution,” in *Proc. Int. Conf. Digital Audio Effects*, 2016, pp. 137–144.

[36] D. Albertini, A. Bernardini, A. Sarti *et al.*, “Antiderivative antialiasing techniques in nonlinear wave digital structures,” in *JAES*, 2021.

[37] M. Holters, “Antiderivative antialiasing for stateful systems,” *Applied Sciences*, vol. 10, p. 20, 2019.

[38] P. P. La Pastina, S. D’Angelo, and L. Gabrielli, “Arbitrary-order IIR Antiderivative Antialiasing,” in *Proc. Int. Conf. Digital Audio Effects*, 2021, pp. 9–16.

[39] M. Otto and J. W. Kurt, “Antiderivative Antialiasing for Recurrent Neural Networks,” in *Proc. Int. Conf. Digital Audio Effects*, 2025.

[40] H. Nyquist, “Certain Topics in Telegraph Transmission Theory,” *Trans. AIEE*, vol. 47, pp. 617–644, 2009.

[41] T. Karras *et al.*, “Alias-Free Generative Adversarial Networks,” *Proc. NeurIPS*, 2021.

[42] J. Schattschneider and U. Zölzer, “Discrete-Time Models for Nonlinear Audio Systems,” in *Proc. Int. Conf. Digital Audio Effects*, 1999, pp. 45–48.

[43] P. Fernández-Cid and J. C. Quirós, “Distortion of Musical Signals by means of Multiband Waveshaping,” *J. New Music Res.*, vol. 30, pp. 279–287, 2001.

[44] L. Ziyin, T. Hartwig, and M. Ueda, “Neural Networks Fail to Learn Periodic Functions and How to Fix It,” *Proc. NeurIPS*, 2020.

[45] Y. Gu, X. Zhang, L. Xue, H. Li, and Z. Wu, “An Investigation of Time-Frequency Representation Discriminators for High-Fidelity Vocoders,” *IEEE/ACM Trans. Audio Speech Lang. Process.*, vol. 32, pp. 4569–4579, 2024.

[46] Y. Gu, X. Zhang, L. Xue, and Z. Wu, “Multi-Scale Sub-Band Constant-Q Transform Discriminator for High-Fidelity Vocoder,” in *Proc. Int. Conf. Acoust. Speech Signal Process.*, 2024, pp. 10616–10620.

[47] H. He *et al.*, “Emilia: An Extensive, Multilingual, and Diverse Speech Dataset for Large-Scale Speech Generation,” in *Proc. IEEE Spoken Lang. Technol. Workshop*, 2024.

[48] —, “Emilia: A Large-Scale, Extensive, Multilingual, and Diverse Dataset for Speech Generation,” *IEEE/ACM Trans. Audio Speech Lang. Process.*, 2025.

[49] Y. Zhang *et al.*, “FoleyCrafter: Bring Silent Videos to Life with Lifelike and Synchronized Sounds,” *arXiv:2407.01494*, 2024.

[50] Y. Gu, R. Zhang, L. Juvela, and Z. Wu, “Solid State Bus-Comp: A Large-Scale and Diverse Dataset for Dynamic Range Compressor Virtual Analog Modeling,” in *Proc. Int. Conf. Digital Audio Effects*, 2025.

[51] Y. Gu, C. Wang, Z. Wu, and L. Juvela, “Neurodyne: Neural Pitch Manipulation with Representation Learning and Cycle-Consistency GAN,” in *Proc. Interspeech*, 2025, pp. 1253–1257.

[52] G. J. Mysore, “Can we Automatically Transform Speech Recorded on Common Consumer Devices in Real-World Environments into Professional Production Quality Speech?—A Dataset, Insights, and Challenges,” *IEEE Signal Process. Lett.*, vol. 22, pp. 1006–1010, 2014.

[53] K. Sodimana *et al.*, “A Step-by-Step Process for Building TTS Voices Using Open Source Data and Frameworks for Bangla, Javanese, Khmer, Nepali, Sinhala, and Sundanese,” in *Proc. SLTU*, 2018, pp. 66–70.

[54] Y. Shi, H. Bu, X. Xu, S. Zhang, and M. Li, “AISHELL-3: A Multi-speaker Mandarin TTS Corpus and the Baselines,” *arXiv:2010.11567*, 2020.

[55] E. Bakhturina, V. Lavrukhin, B. Ginsburg, and Y. Zhang, “Hi-Fi Multi-Speaker English TTS Dataset,” in *Proc. Interspeech*, 2021, pp. 2776–2780.

[56] P. Puchtler, J. Wirth, and R. Peinl, “HUI-Audio-Corpus-German: A High Quality TTS Dataset,” in *Proc. KI*, vol. 12873, 2021, p. 204.

[57] C. Veaux, J. Yamagishi, K. MacDonald *et al.*, “CSTR VCTK corpus: English Multi-speaker Corpus for CSTR Voice Cloning Toolkit (version 0.92),” *CSTR*, 2017.

[58] J. Meyer *et al.*, “BibleTTS: a large, high-fidelity, multi-lingual, and uniquely African speech corpus,” in *Proc. Interspeech*, 2022, pp. 2383–2387.

[59] J. Richter *et al.*, “EARS: An Anechoic Fullband Speech Dataset Benchmarked for Speech Enhancement and Dereverberation,” in *Proc. Interspeech*, 2024, pp. 4873–4877.

[60] M. F. Qharabagh, Z. Dehghanian, and H. R. Rabiee, “ManaTTS Persian: a recipe for creating TTS datasets for lower resource languages,” in *Proc. ACL*, 2025, pp. 9177–9206.

[61] Z. Duan, H. Fang, B. Li, K. C. Sim, and Y. Wang, “The NUS sung and spoken lyrics corpus: A quantitative comparison of singing and speech,” in *Asia-Pac. Signal Inf. Process. Assoc. Annu. Summit Conf.*, 2013, pp. 1–9.

[62] D. A. Black, M. Li, and M. Tian, “Automatic identification of emotional cues in Chinese opera singing,” *Proc. ICMPC*, 2014.

[63] J. Wilkins, P. Seetharaman, A. Wahl, and B. Pardo, “VocalSet: A Singing Voice Dataset,” in *Proc. ISMIR*, 2018, pp. 468–474.

[64] R. Sonobe, S. Takamichi, and H. Saruwatari, “JSUT corpus: free large-scale Japanese speech corpus for end-to-end speech synthesis,” *arXiv:1711.00354*, 2017.

[65] R. Gong, R. Caro, Y. Yang, and X. Serra, “Jingju a Cappella Recordings Collection (Version 2.0),” *10.5281/zenodo.6536490*, 2022.

[66] J. Koguchi, S. Takamichi, and M. Morise, “PJS: phoneme-balanced Japanese singing-voice corpus,” in *Asia-Pac. Signal Inf. Process. Assoc. Annu. Summit Conf.*, 2020, pp. 487–491.

[67] S. Choi, W. Kim, S. Park, S. Yong, and J. Nam, “Children’s song dataset for singing voice research,” in *Proc. ISMIR*, vol. 4, 2020.

[68] H. Tamaru, S. Takamichi, N. Tanji, and H. Saruwatari, “JVS-MuSiC: Japanese multispeaker singing-voice corpus,” *arXiv:2001.07044*, 2020.

[69] J. Shi *et al.*, “Muskits: an End-to-end Music Processing Toolkit for Singing Voice Synthesis,” in *Proc. Interspeech*, 2022, pp. 4277–4281.

[70] R. Huang, F. Chen, Y. Ren, J. Liu, C. Cui, and Z. Zhao, “Multi-Singer: Fast Multi-Singer Singing Voice Vocoder With A Large-Scale Corpus,” in *Proc. ACM MM*, 2021, pp. 3945–3954.

[71] B. Sharma, X. Gao, K. Vijayan, X. Tian, and H. Li, “NHSS: A speech and singing parallel database,” *Speech Commun.*, vol. 133, pp. 9–22, 2021.

[72] J. Liu, C. Li, Y. Ren, F. Chen, and Z. Zhao, “Diff-Singer: Singing Voice Synthesis via Shallow Diffusion Mechanism,” in *Proc. AAAI*, 2022, pp. 11 020–11 028.

[73] J. Liu, C. Li, Y. Ren, Z. Zhu, and Z. Zhao, “Learning the Beauty in Songs: Neural Singing Voice Beautifier,” in *Proc. ACL*, 2022, pp. 7970–7983.

[74] Y. Wang *et al.*, “Opencpop: A High-Quality Open Source Chinese Popular Song Corpus for Singing Voice Synthesis,” in *Proc. Interspeech*, 2022, pp. 4242–4246.

[75] L. Zhang *et al.*, “M4Singer: A Multi-Style, Multi-Singer and Musical Score Provided Mandarin Singing Corpus,” in *Proc. NeurIPS*, 2022.

[76] S. Dai, Y. Wu, S. Chen, R. Huang, and R. B. Dannenberg, “SingStyle111: A Multilingual Singing Dataset With Style Transfer,” in *Proc. ISMIR*, 2023, pp. 765–773.

[77] M. Zheng, P. Bai, X. Shi, X. Zhou, and Y. Yan, “FT-GAN: Fine-Grained Tune Modeling for Chinese Opera Synthesis,” in *Proc. AAAI*, 2024, pp. 19 697–19 705.

[78] J. Shi *et al.*, “Singing Voice Data Scaling-up: An Introduction to ACE-Opencpop and ACE-KiSing,” in *Proc. Interspeech*, 2024.

[79] Y. Gu *et al.*, “SingNet: Towards a Large-Scale, Diverse, and In-The-Wild Singing Voice Dataset,” *arXiv:2505.09325*, 2025.

[80] O. Romani Picas *et al.*, “A real-time system for measuring sound goodness in instrumental sounds,” in *Proc. AES*, vol. 138, 2015.

[81] R. M. Bittner, J. Salamon, M. Tierney, M. Mauch, C. Cannam, and J. P. Bello, “MedleyDB: A Multitrack Dataset for Annotation-Intensive MIR Research,” in *Proc. ISMIR*, 2014, pp. 155–160.

[82] Z. Rafii, A. Liutkus, F.-R. Stöter, S. I. Mimalakis, and R. Bittner, “MUSDB18-HQ-an uncompressed version of MUSDB18,” *Zenodo*, 2019.

[83] E. Manilow, G. Wichern, P. Seetharaman, and J. L. Roux, “Cutting Music Source Separation Some Slakh: A Dataset to Study the Impact of Training Data Quality and Quantity,” in *IEEE Workshop Appl. Signal Process. Audio Acoust.*, 2019, pp. 45–49.

[84] J. Turian, J. Shier, G. Tzanetakis, K. McNally, and M. Henry, “One billion audio sounds from GPU-enabled modular synthesis,” in *Proc. Int. Conf. Digital Audio Effects*, 2021, pp. 222–229.

[85] I. Pereira, F. Araújo, F. Korzeniowski, and R. Vogl, “MoisesDB: A Dataset for Source Separation Beyond 4-Stems,” in *Proc. ISMIR*, 2023, pp. 619–626.

[86] S. Hershey *et al.*, “The Benefit of Temporally-Strong Labels in Audio Event Classification,” in *Proc. Int. Conf. Acoust. Speech Signal Process.*, 2021, pp. 366–370.

[87] R. Ardila *et al.*, “Common Voice: A Massively-Multilingual Speech Corpus,” in *Lang. Resour. Eval.*, 2020, pp. 4218–4222.

[88] Y. Zhang *et al.*, “GTSinger: A Global Multi-Technique Singing Corpus with Realistic Music Scores for All Singing Tasks,” in *Proc. NeurIPS*, 2024.

[89] I. Ogawa and M. Morise, “Tohoku kiritan singing database: A singing database for statistical parametric singing synthesis using Japanese pop songs,” *Acoust. Sci. Technol.*, vol. 42, pp. 140–145, 2021.

[90] J. Salamon, C. Jacoby, and J. P. Bello, “A Dataset and Taxonomy for Urban Sound Research,” in *Proc. ACM MM*, 2014, pp. 1041–1044.

[91] K. J. Piczak, “ESC: Dataset for Environmental Sound Classification,” in *Proc. ACM MM*, 2015, pp. 1015–1018.

[92] I. Martín-Morató and A. Mesaros, “What is the ground truth? Reliability of multi-annotator data for audio tagging,” in *Eur. Signal Process. Conf.*, 2021, pp. 76–80.

[93] R. Sato and J. O. Smith III, “Aliasing Reduction in Neural Amp Modeling by Smoothing Activations,” in *Proc. Int. Conf. Digital Audio Effects*, 2025.

[94] D. Xin, X. Tan, S. Takamichi, and H. Saruwatari, “BigCodec: Pushing the Limits of Low-Bitrate Neural Speech Codec,” *arXiv:2409.05377*, 2024.

[95] X. Zhang *et al.*, “Amphion: an Open-Source Audio, Music, and Speech Generation Toolkit,” in *Proc. IEEE Spoken Lang. Technol. Workshop*, 2024, pp. 879–884.

[96] —, “Leveraging Diverse Semantic-Based Audio Pre-trained Models for Singing Voice Conversion,” in *Proc. IEEE Spoken Lang. Technol. Workshop*, 2024, pp. 758–765.

[97] W.-C. Huang, E. Cooper, and T. Toda, “SHEET: A Multi-purpose Open-source Speech Human Evaluation Estimation Toolkit,” in *Proc. Interspeech*, 2025, pp. 2355–2359.

[98] K. Kilgour, M. Zuluaga, D. Roblek, and M. Sharifi, “Fréchet Audio Distance: A Reference-Free Metric for Evaluating Music Enhancement Algorithms,” in *Proc. Interspeech*, 2019, pp. 2350–2354.

[99] A. Gui, H. Gamper, S. Braun, and D. Emmanouilidou, “Adapting Frechet Audio Distance for Generative Music Evaluation,” in *Proc. Int. Conf. Acoust. Speech Signal Process.*, 2024, pp. 1331–1335.

[100] M. Chinen, F. S. C. Lim, J. Skoglund, N. Gureev, F. O’Gorman, and A. Hines, “ViSQOL v3: An Open Source Production Ready Objective Speech and Audio Metric,” in *Proc. QoMEX*, 2020, pp. 1–6.

[101] M. Schoeffler *et al.*, “A Comprehensive Framework for Web-based Listening Tests,” *J. Open Source Softw.*, vol. 6, no. 1, 2018.

[102] M. Tancik *et al.*, “Fourier Features Let Networks Learn High Frequency Functions in Low Dimensional Domains,” in *Proc. NeurIPS*, 2020.

TABLE VII: Statistics of the speech training and evaluation datasets sorted by their published years.

Dataset	Data Source	Dur. (hour)	Lang.	Samp. Rate (Hz)
DAPS	Studio Recording	67.5	EN	44.1k
HQ-TTS	Studio Recording	191.0	Bangla/Javanese/Khmer Nepali/Sinhala/Sundanese	44.1k
AIShell 3	Studio Recording	85.0	ZH	44.1k
HiFi-TTS	Audio Books	291.6	EN	44.1k
HUI-TTS	Studio Recording	326.0	DE	44.1k
VCTK	Studio Recording	80.0	EN	96k
Bible-TTS	Audio Books	420.3	African Languages	48k
EARS	Studio Recording	100.0	EN	48k
Mana-TTS	Studio Recording	100.0	Persian	44.1k
Common Voice	Studio Recording	5626.0	EN/ZH/JA KO/FR/DE	44.1k
Hitsugi	Studio Recording	0.4	JA	48k
ZunzunProject	Studio Recording	18.9	JA	96k
Voice Seven	Studio Recording	42.6	JA	96k
Coeiroink	Studio Recording	0.6	JA	48k
Amitaro	Studio Recording	5.9	JA	44.1k
Narakuyui	Studio Recording	0.7	JA	48k
Matsukane	Studio Recording	1.5	JA	96k

TABLE VIII: Statistics of the music training and evaluation datasets sorted by their published year.

Dataset	Data Source	Dur. (hour)	Samp. Rate (Hz)
GoodSounds	Studio Recording	28.0	44.1k
MedleyDB	Multi-Track Projects	402.9	44.1k
MUSDB18	Multi-Track Projects	49.1	44.1k
Slakh2100	Kontact Sound Libraries	1680.1	44.1k
Surge Synth	Synthesizers	3.4	44.1k
Arturia Synth	Synthesizers	0.7	44.1k
DX7 Synth	Synthesizers	22.5	44.1k
MoisesDB	Multi-Track Projects	156.4	44.1k
Cambridge Multi-Track	Multi-Track Projects	783.1	44.1k
Cambridge Unmastered	Multi-Track Projects	14.4	44.1k
Internal Dataset	Sample Packs	/	44.1k

TABLE IX: Statistics of the audio training and evaluation datasets sorted by their published year.

Dataset	Data Source	Dur. (hour)	Samp. Rate (Hz)
AudioSet-Strong	In-The-Wild	296.0	44.1k
BBC Effects	In-The-Wild	232.0	44.1k
FreeSound	In-The-Wild	1283.0	44.1k
UrbanSound8K	In-The-Wild	9.0	44.1k
ESC50	In-The-Wild	3.0	44.1k
MACS	In-The-Wild	11.0	44.1k
Internal Dataset	Sample Packs	/	44.1k

TABLE X: Statistics of the singing voice training and evaluation datasets sorted by their published years.

Dataset	Data Source	Dur. (hour)	Style	Lang.	Samp. Rate (Hz)
NUS-48E	Studio Recording	2.8	Children/Pop	EN	44.1k
Opera	Studio Recording	2.6	Opera	IT/ZH	44.1k
VocalSet	Studio Recording	8.8	Opera	EN	44.1k
JSUTSong	Studio Recording	0.4	Children	JA	48k
JaCRC	Studio Recording	28.6	Opera	ZH	44.1k
PJS	Studio Recording	0.5	Pop	JA	48k
CSD	Studio Recording	4.6	Children	EN/KO	44.1k
JVS-Music	Studio Recording	30.0	Children	JA	48k
KiSing	Studio Recording	0.9	Pop	ZH	44.1k
OpenSinger	Studio Recording	51.8	Pop	ZH	44.1k
NHSS	Studio Recording	4.1	Pop	EN	48k
PopCS	Studio Recording	5.9	Pop	ZH	44.1k
PopBuTFy	Studio Recording	30.7	Pop	EN	44.1k
Opencpop	Studio Recording	5.2	Pop	ZH	44.1k
Internal Dataset	Studio Recording	5.2	Pop	ZH	44.1k
M4Singer	Studio Recording	29.7	Pop	ZH	48k
SingStyle111	Studio Recording	12.8	Children/Folk/Jazz Opera/Pop/Rock	EN/IT/ZH	44.1k
GOAT	Studio Recording	4.5	Opera	ZH	48k
ACESinger	SVS	321.8	Pop	EN/ZH	48k
SingNet-SP	Sample Pack	334.3	EDM/Folk/Jazz Opera/Pop/Rap	AR/DE/ES/EN FR/ID/PT/RU ZH/MIS	44.1k
GTSinger	Studio Recording	80.6	Children/Folk/Jazz Opera/Pop/Rock	EN/ZH/JA KO/RU/ES FR/DE/IT	44.1k
Kiritan	Studio Recording	1.2	Pop	JA	96k
Namine Ritsu	Studio Recording	14.4	Pop	JA	44.1k
Voice Seven	Studio Recording	7.2	Pop	JA	96k
Oniku Kurumi	Studio Recording	1.5	Pop	JA	96k
Ofutonp	Studio Recording	1.0	Children	JA	96k
Yuuri Natsume	Studio Recording	1.4	Pop	JA	48k
Amaboshi Cipher	Studio Recording	3.1	Children	JA	44.1k